Nanoscale In Situ Morphological Study of Proteins Immobilized on Gold Thin Films

Francesca A. Scaramuzzo,[†] Romina Salvati,[†] Barbara Paci,[‡] Amanda Generosi,[‡] Valerio Rossi-Albertini,[‡] Alessandro Latini,[†] and Mario Barteri*,[†]

Dipartimento di Chimica, Sapienza Università di Roma, Piazzale A.Moro, 5 - Roma 00185, Italy, and Istituto di Struttura della Materia, C.N.R., Via Fosso del Cavaliere 100 - Roma 00133, Italy

Received: July 27, 2009; Revised Manuscript Received: October 2, 2009

The nanoscale organization of acetylcholinesterase (AChE) and of its polyclonal antibody immobilized on gold thin films was studied by means of Energy Dispersive X-ray Reflectometry (EDXR) and Atomic Force Microscopy (AFM). The macromolecules were alternatively deposited over a self-assembled monolayer (SAM) of *N*-hydroxysuccinimide esters of thioctic acid. The measurements, collected in situ at subsequent deposition stages of the device, gave information on the distribution of the macromolecules on the surface showing that both the proteins can bind covalently to the SAM. In addition to this, we demonstrated that the antigen−antibody reaction takes place when one of the two reactants is anchored to the surface.

Introduction

Acetylcholinesterase (AChE, acetylcholine hydrolase, EC. 3.1.1.7) is an important enzyme of the central nervous system involved in the cholinergic activity of synapses. The principal biological role of AChE is the termination of impulse transmission at cholinergic synapses by rapid hydrolyses of the neurotransmitter acetylcholine (ACh) in acetic acid and choline (Ch). In keeping with this requirement, AChE has a remarkably high specific activity and a rate approaching that of a diffusion-controlled reaction.[1,2]

AChE has been used in biosensors for the detection of insecticides employed in agriculture.[3−5] These products contain molecules able to inhibit AChE covalently binding the Ser residue of its active site.[6,7] On the other hand, some of the AChE inhibitors are used as a remedy in the treatment of various disorders, such as myasthenia gravis, glaucoma, and Alzheimer's disease.[8] In particular, the treatment of Alzheimer's disease is often based on the use of AChE inhibitors, i.e., tacrine, to reduce neurological impairments. However, a critical point of pharmacological treatment is to establish the correct dose of inhibitors to avoid the so-called paradox effect, which provides an increase, instead of a reduction, of the symptoms. Thus, AChE-based biosensors may be useful tools to determine the concentration of residual drug in the blood and to optimize pharmacological therapy.

Several different methods to design specific recognition systems have already been described, showing that the sensitivity of a biosensor depends on the efficiency and on the concentration of the bioactive compound used (bioreceptor). For AChE, it should be mentioned that the pioneering work of George G. Guilbault focused on purification, inhibition analysis,[9−11] immobilization,[12] and development of activity assay of cholinesterases.[13−15]

In this paper we discuss the physical chemical characterization of the antigen−antibody (AChE and its polyclonal antibody AbAChE) interaction on the metallic surface. Experimental data obtained demonstrate that in spite of the immobilization the proteins did not change their capability of undergoing the immunochemical reaction.

Experimental Methods

Gold thin films with controlled thickness, crystalline structure, and the highest possible degree of flatness were obtained by physical vapor deposition performed inside a stainless steel high vacuum chamber evacuated by a turbo molecular pump (vacuum better than 5×10^{-5} mbar). The film deposition protocol was as follows: first, a 100 nm thick chromium layer was deposited on glass microscope slides using a beam accelerated at −3.5 kV with a current intensity of 40−50 mA (deposition rate 0.2−0.5 nm/s); then a 100 nm gold layer was deposited using a beam accelerated at −5 kV with a current intensity of about 100 mA (deposition rate 0.1−0.2 nm/s). The Cr layer between glass and gold was required to overcome the problem of the very poor adhesion of gold films on most surfaces, including glass.

The SAMs were constituted by 1-{[5-(1,2-dithiolan-3-yl)pentanoyl]oxy}pyrrolidine-2,5-dione (ThA), which is the ester obtained by condensation of thioctic acid and *N*-hydroxysuccinimide (NHS) (Figure 1), using the receipt suggested by Stokes.[16]

The monolayer was prepared by covering the gold film with a 5 mM ThA solution in ethanol/acetic acid 15:1 for 24 h. During this lapse of time, the disulfide group of ThA reacts with gold atoms exposed to the metal−solution interface, gradually determining the self organization of a monomolecular layer of activated esters. To immobilize the proteins, the SAM was made to react with an aqueous solution of AChE or, alternatively, with an aqueous solution of antibody in potassium phosphate buffer (0.1 M, pH 7.0) for 2 h. At this pH, amino groups of the lysine residues of the protein slowly react with ThA[17] bound to the metal surface. The amide formation leads to a covalent and stable anchorage of the protein to the SAM. To avoid nonspecific binding of antibody to surface adjacent to covalently bound antigen and vice versa, after each step of immobilization we rinsed samples with 0.1 M PBS buffer solution containing 0.05% of polysorbate (Twin 20). Polysorbate

* To whom correspondence should be addressed. Phone number: 0039 06 49913957. Fax number: 0039 06 490631. E-mail address: mario.barteri@uniroma1.it.
[†] Sapienza Università di Roma.
[‡] Istituto di Struttura della Materia.

10.1021/jp907149m CCC: $40.75
Published on Web 11/10/2009

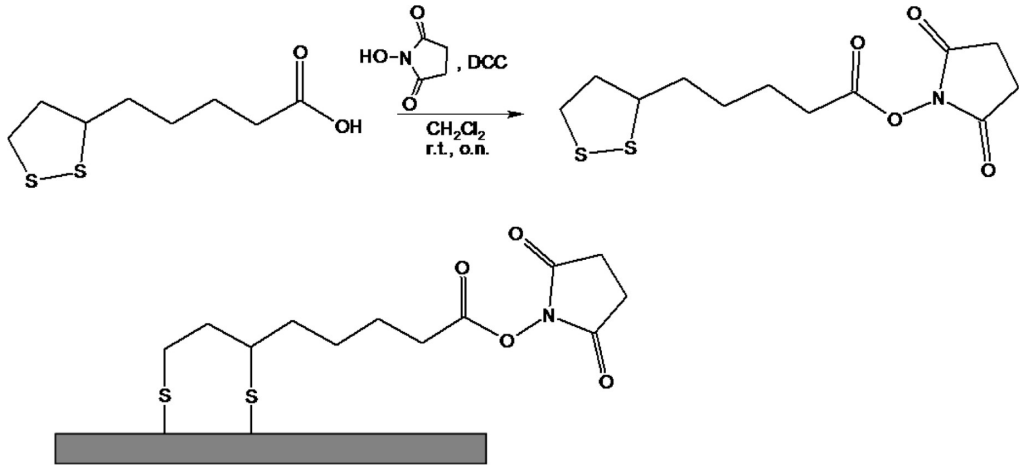

Figure 1. Thioctic acid esterification reaction and schematic representation of ThA assembled on Au.

is a mild surfactant capable of minimizing the hydrophobic protein−protein interactions, particularly strong for antibodies.

X-ray diffraction of the Au layers was performed using a Panalytical X'Pert Pro diffractometer (Bragg-Brentano geometry) at grazing incidence (radiation Cu $K_{\alpha 1} = 0.154056$ nm). Atomic Force Microscopy (AFM) and Energy Dispersive X-ray Reflectometry (EDXR) measurements were carried out in situ on the substrates mentioned above and on the systems at subsequent stages of deposition, allowing a step by step characterization. To collect EDXR measurements, we used a noncommercial machine[18] characterized by a very simple set-up geometry, with neither a monochromator nor a goniometer. We have already demonstrated that the EDXR technique is a powerful tool for investigating thin film layered samples and devices.[19,20] Indeed, since in the ED mode the scan of the reciprocal space is carried out electronically, rather than mechanically as in conventional X-ray diffraction,[21,22] the set-up is kept in static conditions during the measurements. Therefore, both the scattering volume of the film and the footprint of the X-ray beam on the film surface are constant, which makes data analysis simpler and more reliable. The machine consists of an X-ray tube and an energy sensitive detector, mounted on two benches pivoting around a common central axis. In this way, systematic errors induced by repositioning of the diffractometer arms, critical when measurements are performed at grazing incidence, are prevented.

The X-ray optical path is defined by four adjustable slits. The bremsstrahlung of the 3 kW tungsten anode X-ray tube is used as a probe, while the energy scan is performed by an EG&G high purity germanium solid-state detector, with energy resolution of about 1.5−2% in the 15−50 keV energy range. From the experimental curves, all collected at a grazing scattering angle of $\theta = 0.140°$, we obtained the numeric value of the scattering parameter q at the critical reflection edge (q_c)

$$q_c = 2\sqrt{4\pi\rho_e}$$

where ρ_e is the film scattering length density (proportional to the material density in the scattering volume). The best fit of the total reflection edge can be calculated using the Porod approximation. On the other hand, the roughness of the sample, determining the pattern slope, is obtained by applying the Parratt formula[18,23] to fit the linear part of the curve.

Results

X-ray measurements of the Au layer show that the films have a preferential crystalline Au (111) orientation (Figure 2). Figure

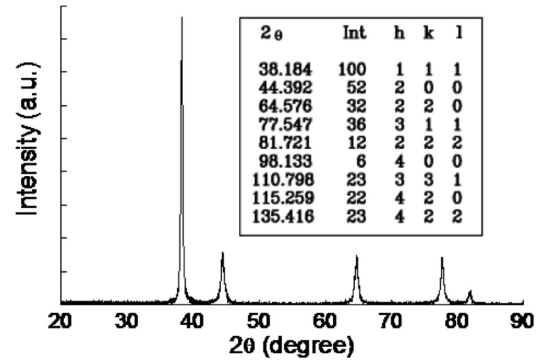

Figure 2. X-ray diffraction pattern of Au thin film prepared by means of physical vapor deposition on glass.

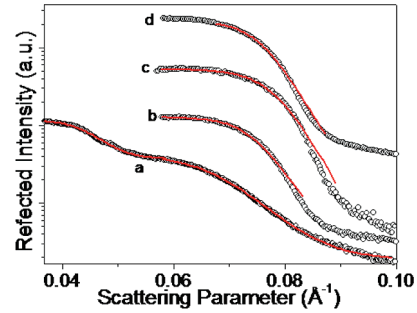

Figure 3. X-ray reflectivity profiles, shifted in high for clarity, collected at a scattering angle of $\theta = 0.140°$ upon the various steps of the deposition of the device: Au substrate (a), ThA-coated Au (b), immobilized AChE (c), and Au−ThA−AChE−AbAChE complex (d).

3 shows the in situ EDXR patterns at the subsequent stages of deposition. The pattern corresponding to the substrate (curve a) reveals the presence of a double edge generated by the total reflection of the Cr layer and the total reflection of the Au film deposited upon it, respectively, at $q_c(\mathrm{Cr}) = 0.048$ Å^{-1} and $q_c(\mathrm{Au}) = 0.072$ Å^{-1}. The reflectivity patterns of the Au samples functionalized, respectively, with the SAM of ThA (curve b), with AChE covalently bound to the SAM of ThA (curve c), and with the complex ThA−AChE−AbAChE (curve d) are also reported. Table 1 summarizes the experimental results.

The deposition of the ThA molecules on the Au film induces the progressive formation of the SAM layer on the surface. Since the total reflection edge q_c is related to the material density, its position changes upon the progressive binding of the ThA molecules on the Au surface, approaching the asymptotic value

TABLE 1: Critical Values of the Scattering Parameter q_c, Scattering Length Density ρ_e, and Roughness σ of the Au Film, ThA-Coated Au, Immobilized AChE, and Au−ThA−AChE−AbAChE Complex[a]

sample	q_c (Å^{-1}) 10^2	ρ_e (Å^{-2}) 10^4	σ (Å)	σ_{AFM} (Å)
Au	7.2 ± 0.1	1.03 ± 0.05	5 ± 1	10 ± 5
Au−ThA	7.5 ± 0.1	1.10 ± 0.05	10 ± 1	24 ± 5
Au−ThA−AChE	8.1 ± 0.1	1.30 ± 0.05	17 ± 1	28 ± 5
Au−ThA−AChE−AbAChE	7.8 ± 0.1	1.20 ± 0.05	13 ± 1	22 ± 5

[a] The roughness value obtained by the AFM analysis, σ_{AFM}, is also reported for comparison.

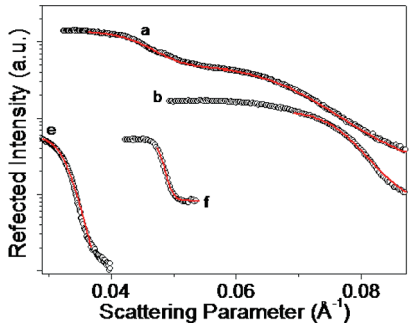

Figure 4. X-ray reflectivity profiles, shifted in high for clarity, collected at a scattering angle of $\theta = 0.140°$ upon the various steps of the deposition of the device: Au substrate (a), ThA-coated Au (b), immobilized AbAChE (e), and Au−ThA−AbAChE−AChE complex (f).

TABLE 2: EDXR and AFM Physical Parameters Obtained as in Table 1 for Au Film, ThA-Coated Au, Immobilized AbAChE, and Au−ThA−AbAChE−AChE Complex

sample	q_c (Å^{-1}) 10^2	ρ_e (Å^{-2}) 10^4	σ (Å)	σ_{AFM} (Å)
Au	7.2 ± 0.1	1.03 ± 0.05	5 ± 1	10 ± 5
Au−ThA	7.5 ± 0.1	1.10 ± 0.05	10 ± 1	24 ± 5
Au−ThA−AbAChE	3.3 ± 0.1	0.22 ± 0.05	20 ± 1	34 ± 5
Au−ThA−AbAChE−AChE	4.8 ± 0.1	0.46 ± 0.05	18 ± 1	30 ± 5

reported in Table 1. Moreover, the formation of the SAM layer gives rise to an increase of the surface roughness (about 100%), detected as a variation of the slope of the reflectivity curves. A similar behavior occurs at the subsequent stage of device fabrication, the Au−ThA−AChE system, showing a further increase in both the q_c and the σ parameters (roughness increases of a further 70%). Actually, in the perspective of setting up a device for the AChE detection, we tested the reactivity of AChE on the immobilized AbAChE. Thus, a new series of samples of immobilized AbAChE were prepared and characterized, to verify the reaction between anchored antibody and antigen (AChE) in buffered water solution. In Figure 4, the results obtained for the AbAChE upon the ThA SAM (curve e) and for the ThA-AbAChE−AChE complex (curve f) are shown.

As in Figure 3, curves a and b are referred to the Au film and to the ThA SAM. Table 2 summarizes the experimental results. The EDXR patterns of the Au film and of the ThA SAM (curves a and b) provide the same results obtained in the previous series of samples. AbAChE deposition causes a sensible reduction of the scattering length density and a large roughness increase, while after the addition of AChE a slight decrease of the roughness occurs, as a consequence of the antigen−antibody reaction. Although the enzyme immobilization produces a significant increase in the scattering length density, this value is smaller than that of the former sequence, namely, when the AbAChE reacts with the immobilized enzyme.

In situ AFM measurements performed using a noncommercial air operating atomic force microscope[24] in noncontact mode gave additional information on the biomacromolecule distribution and on their morphology. The AFM experiments on the subsequent stages of the biosensor were performed in the same conditions, using the same tip. Each layer was deposited in situ, opening the microscope head, without removing the sample.

The AFM maps of samples shown in Figure 5 correspond to the subsequent steps of the device deposition: (a) Au substrate; (b) ThA SAM on Au; (c) immobilized AChE on ThA SAM on Au; (d) Au−ThA−AChE−AbAChE complex; (e) immobilized AbAChE on ThA SAM on Au; (f) Au−ThA−AbAChE−AChE complex. In each section, a schematic cartoon of the surface, a 2D AFM image of a (3 μm × 3 μm) magnification field and a 3D AFM image of a (1 μm × 1 μm) magnification field are shown.

The first four sections correspond to patterns a−d of Figure 3, while the last two are related to patterns e−f of Figure 4. After the ThA formation, the overall AFM data collection at different stages of deposition (from Figure 5c to Figure 5d and from Figure 5e to Figure 5f) was performed in a few hours, as the acquisition time for each measurement is of 10−20 minutes. Since the microscope we used is characterized by elevated stability (less than 30 nm drift in 7 h), we can exclude the occurrence of artifacts due to instrumental drift or piezo relaxation. For this reason, all the observed topographical features can be reasonably assigned to the modification of the sample surface.

Such AFM analysis provided detailed images of the coated surface and an independent measurement of the roughness (see Table 1 and Table 2). The roughness value was calculated as the mean square root of the local height fluctuations around the height average value at the surface. This value resulted to be higher in the absence of antigen, as it is also evident comparing the scale amplitude: 44 and 33 nm, respectively, for the images in Figure 5c and 5d.

It is important to notice that the absolute roughness value retrieved by AFM measurements, σ_{AFM},[25] is not directly comparable to that given by EDXR[18,26] for the same sample. Indeed, the former gives a local microscopic image of the direct space, while the latter uses a spectroscopic probe of the reciprocal space to provide a roughness value (variance from the mean average thickness) averaged over the X-ray beam footprint on the sample surface ($2 \times 10\ \mu m^2$). Therefore, EDXR provides the roughness value averaged on a macroscopic area, while AFM explores just small portions of the surface. Processing an AFM image, a local measure of the roughness is obtained. On the other hand, when in situ studies are performed, a limited number of images can be collected in a reasonable measuring time, and the sampling may not be accurate enough to allow a quantitative comparison of the AFM and EDXR data. Therefore, the correct (mean) roughness value is provided only by EDXR. As a consequence, the larger roughness values measured by AFM with respect to those measured by EDXR indicate that topography of the sample portion analyzed by AFM is more irregular than the average of the whole surface. Nevertheless, the information inferred at different deposition stages is that the roughness values obtained with the two different techniques follow the same trend.

Discussion

The changes in the system morphology detected by the EDXR experiments are compatible with a modulation of the film electronic density and roughness induced by the prior formation of the ThA

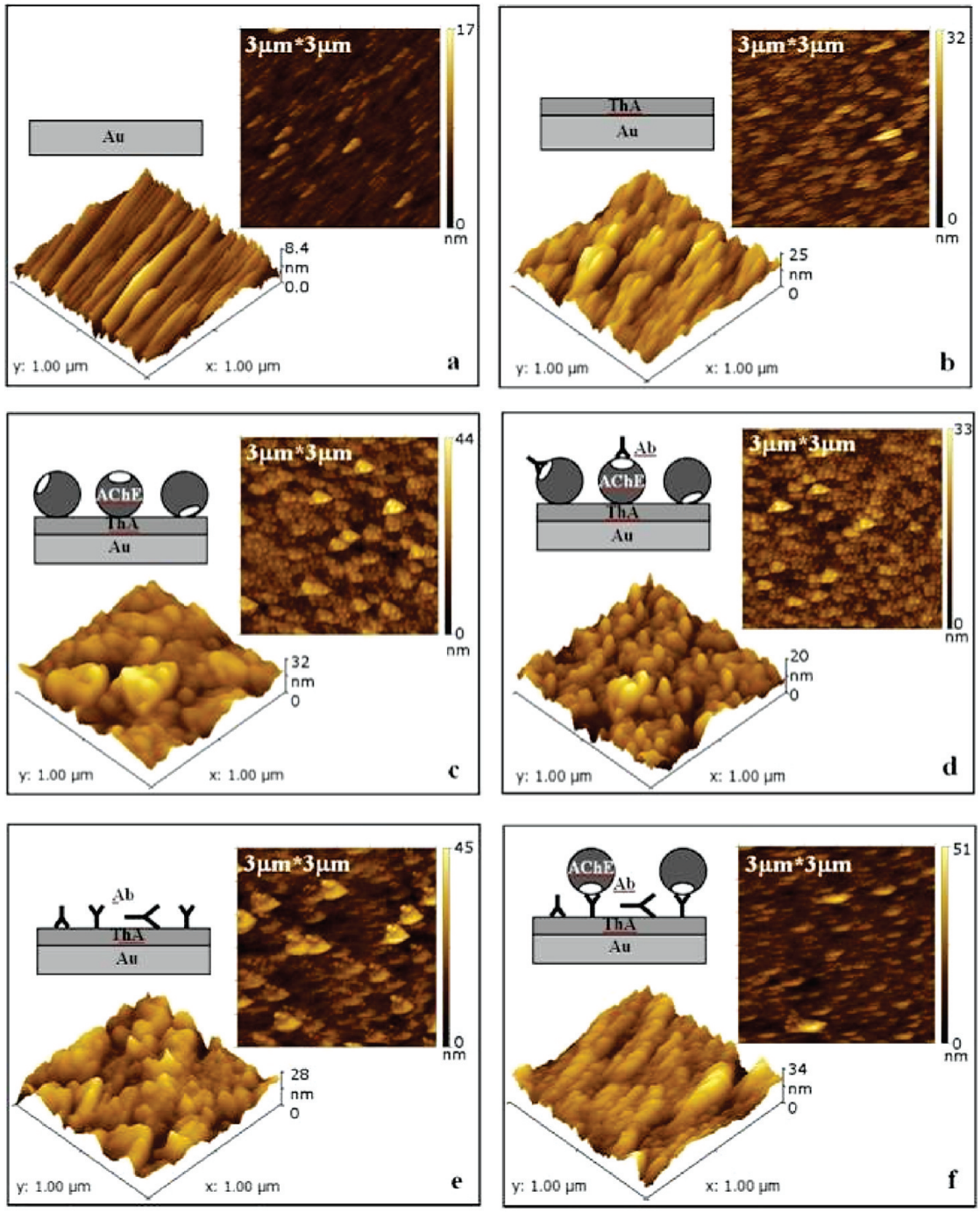

Figure 5. AFM maps collected on samples at different steps of the device deposition: (a) Au substrate, (b) ThA-coated Au, (c) immobilized AChE on ThA-coated Au, (d) ThA−AChE−AbAChE complex, (e) immobilized AbAChE on ThA-coated Au, and (f) Au−ThA−AbAChE−AChE complex. The first four images refer to the first deposition sequence (patterns a−d in Figure 2) and the last two to the second (inverted) deposition sequence (patterns e−f in Figure 3).

SAM layer and the consequent immobilization of the macromolecules. EDXR data reported in Tables 1 and 2 put in evidence a different trend of q_c and ρ_e when the deposition order of AChE and AbAChE is alternated; such differences can be attributed to the different shape and molecular weight of the two macromolecules. In fact, the antibody has a typical Y shape and a molecular weight of about 67 kDa, while AChE is a dimer with a globular shape and a molecular weight of 160 kDa. Since the immobilization of both the proteins on the surface does not have a preferential orientation, these differences are crucial in the anchoring process in terms of coating extension and in the subsequent antigen−antibody reaction. In particular, immobilization of AChE leads to an increase of electronic density (by EDXR) and local and averaged roughness (determined, respectively, with AFM and X-ray measurements). Because of the AChE globular structure, there is a high probability of epitope exposure towards the solvent, where the antibody is dissolved, thus facilitating the immunochemical reaction. In this way, the highly specific antigen−antibody interaction takes place on enzyme molecules anchored without any preferential orientation. Furthermore, the formation of the antigen−antibody complex reduces the intermolecular spaces among the immobilized enzyme molecules, determining a decrease of q_c, ρ_e, and σ.

As for AChE, the immobilization of the antibody on ThA occurs without any preferential orientation, but it provides a decrease of electronic density. To explain this different behavior, it should be considered that the immobilization of the proteins on the ThA SAM is due to the formation of an amide involving the amino groups of the side chains of the lysine residues on the biomolecule and the activated esters on the surface. The Y shape of the antibody gives rise to modes of binding different from those of a globular-shaped protein because of the different number and distribution of lysine residues. As a consequence, both the heavy and the light chains can interact with the surface, as schematically represented in the cartoon of Figure 5e. Therefore, the binding of the antibody to the surface results in a layer more disordered than the AChE one. Such a disorder causes a decrease of the number of atoms (and, as a consequence, of electrons) in the scattering volume closest to the metal surface. Among all the possible antibody orientations on the surface, only those which expose the light chains toward the solvent are suitable to the AChE binding.

The comparison of EDXR and AFM results, retrieved over the series of samples investigated, shows that the trends of the roughness modifications are in good agreement. Figure 5b shows the morphology of the ThA layer coated surface, characterized by elongated repetition units of ellipsoidal shape aligned along the diagonal image plane. This feature reveals remarkable differences if compared to the bare gold. An increase in the surface roughness is also observed, in agreement with the corresponding EDXR measurements, as reported in Table 1. In Figure 5c the immobilized AChE enzyme appears like well-defined triangular features with spherical substructures, which cause a further increase of the surface roughness. As the device is completed by deposition of the AbAChE, a similar diffuse granular texture appears amidst the triangular structures (Figure 5d). In this case, the roughness is reduced by the presence of the antibody which can fill the intermolecular spaces among the immobilized enzyme molecules, as already hypothesized to explain EDXR measurements. The AFM analysis of immobilized AbAChE reveals partially overlapped structures of irregular shape and variable size, with a preferential orientation along the diagonal of the image but without particular internal substructures (Figure 5e). Finally, the reaction between AChE and its polyclonal antibody provides a morphology with an extremely regular texture (Figure 5f). The ThA−AbAChE layer is covered by parallel ellipsoidal granular structures with stripelike substructures orthogonal to the major axis of the ellipsoidal objects themselves. Once more, a slight decrease of the roughness is observed, confirming the same trend of the EDXR measurements. These data suggest that the deposition of AChE on AbAChE allows a very homogeneous distribution of the macromolecules on the final device surface, which is an essential goal to achieve for biosensor applications. In fact, it is well known that the inhomogeneous deposition of bioreceptor is the main reason for poor reproducibility observed comparing biosensors with different grades of enzyme coating.[27,28]

Conclusions

In this paper, we proposed a protocol to carry out an accurate analysis of a protein deposition process on thin gold layers. To sum up, both the innovative EDXR and AFM set-ups used for this study give the possibility of collecting data keeping the sample in air, thus simplifying the experimental modus operandi. This kind of instrumentation allowed us to perform a step by step characterization of the process of protein assembly on the thin film at nanometric scale, which should be considered a preliminary procedure for biosensor design.

References and Notes

(1) Hasinoff, B. B. *Biochim. Biophys. Acta* **1982**, *704*, 52–8.
(2) Bazelyansky, M.; Robey, E.; Kirsch, J. F. *Biochemistry* **1986**, *25*, 125–130.
(3) Moulton, C. A.; Fleming, W. J.; Purnell, C. E. *Environ. Toxicol. Chem.* **1996**, *15*, 131–137.
(4) Sheets, L. P.; Hamilton, B. F.; Sangha, G. K.; Thyssen, J. H. *Fundam. Appl. Toxicol.* **1997**, *35*, 101–119.
(5) Marrs, T. C. *Pharmacol. Ther.* **1993**, *58*, 51–66.
(6) Schulze, H.; Vorlová, S.; Villatte, F.; Bachmann, T. T.; Schmid, R. D. *Biosens. Bioelectron.* **2003**, *18*, 201–209.
(7) Quinn, D. M. *Chem. Rev.* **1987**, *87*, 955–979.
(8) *The Pharmacological Basis of Therapeutics*; Taylor, P., Gilman, A. G., Rall, T. W., Nies, A., Taylor, P., Eds.; Pergamon: New York, 1990; pp 131−149.
(9) Guilbault, G. G.; Das, J. *Anal. Biochem.* **1970**, *33*, 341–355.
(10) Guilbault, G. G.; Iwase, A. *Anal. Chim. Acta* **1976**, *85*, 295–300.
(11) Guilbault, G. G.; Kramer, D. N. *Anal. Chem.* **1965**, *37*, 1675–1680.
(12) Guilbault, G. G.; Kuan, S. S.; Tully, J.; Hackney, D. *Anal. Biochem.* **1970**, *36*, 72–77.
(13) Guilbault, G. G.; Sadar, M. H.; Kuan, S. S.; Casey, D. *Anal. Chim. Acta* **1970**, *51*, 83–93.
(14) Guilbault, G. G.; Sadar, M. H.; Kuan, S. S.; Casey, D. *Anal. Chim. Acta* **1970**, *52*, 75–82.
(15) Guilbault, G. G.; Schmid, R. D.; Turner, A. P. F.; Yevdokimov, Y. M. *Adv. Biosens.* **1991**, 257–289.
(16) Stokes, R. J.; Macaskill, A.; Dougan, J. A.; Hargreaves, P. G.; Stanford, H. M.; Smith, W. E.; Faulds, K.; Graham, D. *Chem. Commun.* **2007**, *27*, 2811–2813.
(17) Vaughan, R. D.; O'Sullivan, C. K.; Guibault, G. G. *Fresnius J. Anal. Chem.* **1999**, *364*, 54–57.
(18) Rossi Albertini, V.; Paci, B.; Generosi, A. *J. Phys. D, Appl. Phys.* **2006**, *39*, 461–486.
(19) Rossi Albertini, V.; Generosi, A.; Paci, B.; Perfetti, P.; Rossi, G.; Capobianchi, A.; Caminiti, R. *Appl. Phys. Lett.* **2003**, *8222*, 3868–3868.
(20) Paci, B.; Generosi, A.; Rossi Albertini, V.; Perfetti, P.; de Bettignies, R.; Firon, M.; Leroy, J.; Sentein, C. *Appl. Phys. Lett.* **2006**, *89*, 043507−043510.
(21) Paci, B.; Generosi, A.; Rossi Albertini, V.; Perfetti, P.; de Bettignies, R.; Firon, M.; Leroy, J.; Sentein, C. *Appl. Phys. Lett.* **2005**, *87*, 194110–194112.
(22) James, R. W. *The Optical Principles of the Diffraction of X-ray*; OX BOW Press: Woodbridge, Connecticut, 1982.
(23) Parratt, L. G. *Phys. Rev.* **1954**, *95*, 359–369.
(24) Cricenti, A.; Generosi, R. *Rev. Sci. Instrum* **1995**, *66* (5), 2843–2847.
(25) Sedin, D. L.; Rowlen, K. L. *Appl. Surf. Sci.* **2001**, *182*, 40–48.
(26) Névot, L.; Croce, P. *Rev. Phys. Appl.* **1980**, *15*, 761–779.
(27) Danzer, T.; Schwedt, G. *Anal. Chim. Acta* **1996**, *318*, 275–286.
(28) Chouteau, C.; Dzyadevych, S.; Durrieu, C.; Chovelon, J. M. *Biosens. Bioelectron.* **2005**, *21*, 273–281.

JP907149M